PROCEEDINGS OF SCIENCE

The cosmic-ray electron and positron spectrum measured with CALET on the International Space Station

Yosui Akaike[a,b,*] **and Shoji Torii**[a] **for the CALET collaboration**

[a] *Waseda Research Institute for Science and Engineering, Waseda University, 17 Kikuicho, Shinjuku, Tokyo 162-0044, Japan*

[b] *JEM Utilization Center, Human Spaceflight Technology Directorate, Japan Aerospace Exploration Agency, 2-1-1 Sengen, Tsukuba, Ibaraki 305-8505, Japan*

E-mail: yakaike@aoni.waseda.jp

The CALorimetric Electron Telescope (CALET) has been collecting data on the International Space Station for more than seven years since October 2015. CALET is an all-calorimetric instrument with a total vertical thickness of 30 radiation lengths and fine imaging capability, optimized for the measurement of the electron and positron (all-electron) spectrum well into the TeV energy region. The observed event statistics have increased more than three times since its last publication about the all-electron spectrum to 4.8 TeV in 2018. Based on Monte Carlo simulations, the data analysis effectively rejects background protons, resulting in less than 10% contamination up to the TeV region. The expected systematic errors are investigated. The significance of the cutoff at the TeV region in the energy spectrum, which is expected as a result of radiation loss during propagation, has increased to over 6σ. By observing the detailed structure in the TeV region of the energy spectrum, we will investigate on the presence of possible nearby cosmic-ray sources. In this paper, we will present the updated all-electron spectrum, and briefly discuss its interpretations.

38th International Cosmic Ray Conference (ICRC2023)
26 July - 3 August, 2023
Nagoya, Japan

ICRC2023
38th International Cosmic Ray Conference
The Astroparticle Physics Conference

*Speaker

© Copyright owned by the author(s) under the terms of the Creative Commons Attribution-NonCommercial-NoDerivatives 4.0 International License (CC BY-NC-ND 4.0).

PoS(ICRC2023)071

1. Introduction

It has widely been recognized that the cosmic-ray electrons are accelerated in supernova remnants (SNRs) by the first order Fermi acceleration mechanism with diffusive shock, and lose their energy in proportion to E^2 via synchrotron and inverse Compton scattering during propagation in the Galaxy. As a result, the energy spectrum of electron is expected to become softer at high energies due to the radiation processes. Above 1 TeV, a break of the spectrum is expected since only nearby (<1 kpc) and young ($<10^5$ years) sources can contribute to the flux if the sources are SNRs as it is commonly believed. Such a source like Vela is a few, precise measurement of the electron spectrum in TeV region can identify the specific cosmic-ray sources, and provide direct information on the mechanisms of acceleration and propagation of cosmic rays [1, 2].

In addition, the increase of the positron fraction above 10 GeV, established by the Payload Antimatter Matter Exploration and Light nuclei Astrophysics (PAMELA) [3] and the Alpha Magnetic Spectrometer (AMS-02)[4], requires a primary source component of the positrons in addition to the generally accepted secondary origin. Candidates for such primary sources range from astrophysical (pulsar) to exotic (dark matter). Since these primary sources emit electron-positron pairs, it is expected that the all-electron spectrum would exhibit a spectral feature due to the primary source component of electrons and positrons, in the corresponding energy range above 10 GeV.

The CALorimetric Electron Telescope (CALET) is a space experiment on the International Space Station (ISS) for long term observations of cosmic-rays, which is optimised for the measurement of the all-electron spectrum [5]. It was launched on August 19, 2015 with the Japanese carrier H-IIB, delivered to the ISS by the HTV-5 Transfer Vehicle, and installed on the Japanese Experiment Module - Exposed Facility (JEM-EF). The first result of the all-electron spectrum was published in the energy range from 10 GeV to 3 TeV as the world's first space observation to the TeV region [6]. Subsequently, the updated spectrum was published with statistics larger by a factor of ∼2 compared to the first by using more than two years of flight data and the full geometrical acceptance in the high-energy region [7]. The energy range is extended to 4.8 TeV, and the observed spectrum shows a suppression of the flux above 1 TeV, which is compatible with the DAMPE result [7]. In this paper, we present a preliminary CALET all-electron spectrum with a further increase in statistics by a factor ∼ 3.4 since the last publication [7], using 2637 days of flight data from October 13, 2015 to December 31, 2022. The spectrum integrates 7.02 million electron (+positron).

2. CALET Instrument

CALET is a fully active calorimeter optimized for electron observations from 1 GeV to 20 TeV. It consists of a charge detector (CHD), a 3 radiation-length thick imaging calorimeter (IMC), and a 27 radiation-length thick total absorption calorimeter (TASC). It has a field of view of approximately 45 degrees from zenith and a geometrical factor of 1040 cm^2sr for high-energy electrons. The IMC induced the start of the shower development for electromagnetic particles while suppressing nuclear interactions in order to maximize the proton rejection power for the electron candidates, and provides the direction of incident particles. It is composed of 7 layers of tungsten absorbers interleaved with scintillating fiber (SciFi) belts read-out individually with 64-anode PMTs. The TASC installed below the IMC measures the energy of shower particles caused by the interaction of the incident

PoS(ICRC2023)071

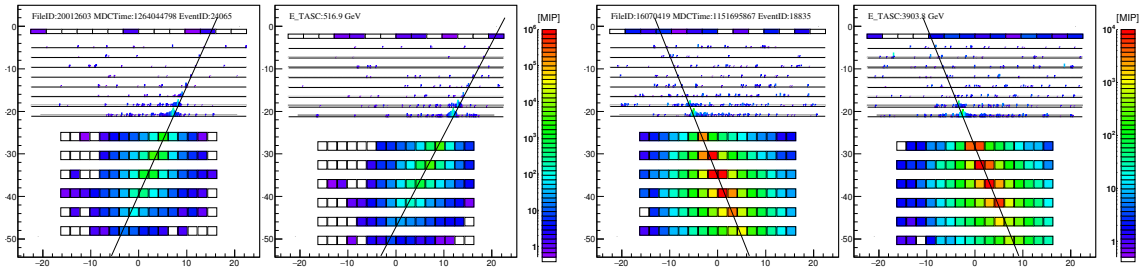

Figure 1: The shower profiles projected onto the X-Z and Y-Z view of electron candidates with an energy deposit sum in TASC of 570 GeV (left) and 3.90 TeV (right). Black lines represent the reconstructed tracks using the shower tracking, which achieves a fine resolution taking advantage of the high granularity of the IMC.

particles in the IMC. It is a tightly packed lead-tungstate ($PbWO_4$; PWO) hodoscope, allowing for a nearly total containment of TeV electron showers. The CHD, placed at the top of the detector to identify the charge of incident particle, is comprised of a pair of plastic scintillator hodoscopes arranged in two orthogonal layers. Figure 1 shows examples of electron candidate with an energy deposit sum in TASC of 570 GeV and 3.90 TeV. Thanks to the thick calorimeter, the shower energy of TeV electrons is fully contained in the detector, with energy resolution of 2% or better in the energy range from 20 GeV to 20 TeV. Since the start of operation, smooth and continuous operations have taken place without any major interruption, and the detector performance is very stable.

3. Data analysis

Events used in this analysis are detected by the high energy, HE, trigger [8] which requires a coincidence of the two bottom layers of IMC and the top layer of TASC. The HE trigger mode always operates. The energy threshold is set to detect electrons above 10 GeV. A Monte Carlo (MC) program was developed to simulate physics processes and detector signals based on the simulation package EPICS [9] with a hadron interaction model of DPMJET-III [10]. It was tuned and tested with accelerator beam test data [11], and a detailed detector configuration was implemented. The MC event samples are generated in order to derive event selection and event reconstruction efficiencies, energy correction factor, and background contamination.

Calibration Energy calibration is essential for CALET as a calorimeter instrument to achieve high precision and accurate measurements. The method of energy calibration and the associated uncertainties have been described elsewhere [12]. Regarding temporal variations occurring during long-term observations, each detector component is calibrated by modeling variations of the minimum ionizing particles (MIP) peak obtained from non-interacting protons and helium recorded with a dedicated trigger mode[8].

Track reconstruction As a track recognition algorithm, we adopt the "electromagnetic shower tracking" [11], which takes advantages of the electromagnetic shower shape and the IMC design concept. Thanks to optimized arrangement of tungsten plates between the SciFi layers, shower cascades are smooth and stable for electron showers. By using the preshower core at the bottom

PoS(ICRC2023)071

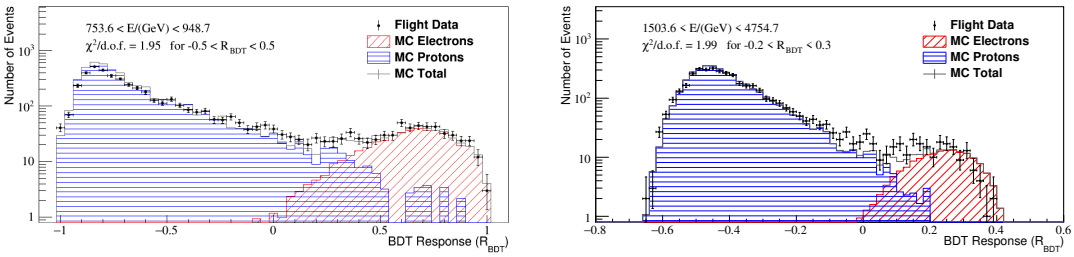

(a) An example of the BDT distribution in the $754 < E < 945$ GeV bin with 9 parameter.

(b) An example of the BDT distribution in the $1.5 < E < 4.8$ TeV bin with 13 parameter.

Figure 2: Examples of BDT response distributions

of the IMC layers as initial track candidates, a very reliable and highly efficient track recognition becomes possible with less energy dependence.

Pre-selection Preselections of well-reconstructed and well-contained single charged events are applied to minimize and accurately subtract proton contamination in the sample of electron candidates. Furthermore, by removing events not included in MC samples, i.e., particles with an incident angle from the zenith angle larger than 90° and heavier particles, equivalent event samples between data and MC calculations were obtained. The preselection consists of (1) an off-line trigger confirmation, which energy threshold is severe than that of onboard threshold for the two layers of the bottom of IMC and the top layer of TASC, (2) geometrical condition, (3) a track quality cut to ensure reconstruction accuracy, (4) charge selection using the CHD, and (5) longitudinal shower development and (6) lateral shower containment consistent with those expected for electromagnetic cascades. The combined efficiency of preselection for electron is $\sim 90\%$.

Energy reconstruction An energy correction function is derived using the electron MC data after preselection. The energy deposit in the detector is obtained as the sum of the TASC and IMC, where a simple sum is sufficient for the TASC, while compensation for energy deposits in tungsten plates is necessary for the IMC. The correction function is then derived by calculating the average ratio of the true energy to the energy-deposit sum in the detector. Because of near total absorption of the shower, the correction factor is very small, ~5%, up to the TeV region. The absolute energy was calibrated and shifted by +3.5% [6] as a result of a study of the geomagnetic cutoff. Since the full dynamic range calibration was carried out with a scale-free method, its validity holds regardless of the absolute scale uncertainty.

Electron identification To identify electrons and to study systematic uncertainties in the electron identification, two methods are applied; a simple two-parameter cut below 476 GeV and a multivariate analysis above. A simple two-parameter cut is embedded into the K estimator defined as $K = \log_{10} F_{\mathrm{E}} + R_{\mathrm{E}}/2$ cm, where R_{E} is the second moment of the lateral energy-deposit distribution in the TASC first layer computed with respect to the shower axis, and F_{E} is the fractional energy deposit of the bottom TASC layer with respect to the total energy deposit sum in the TASC. The latter is based on Boosted Decision Trees (BDTs) optimized in the energy interval below (above) 949 GeV, using 9 (13) parameters, respectively. Calculation of event selection efficiencies, BDT training, and estimation of proton back-ground contamination are carried out separately for each geometrical condition and combined in the end of obtain the final spectrum.

PoS(ICRC2023)071

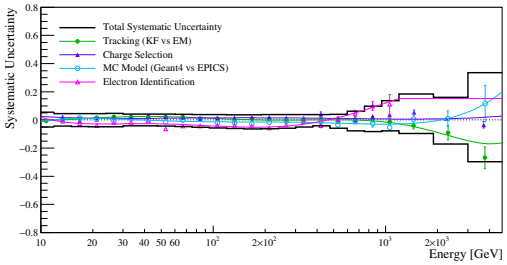

Figure 3: Energy dependence of systematic uncertainties. The solid line represents the total systematic. The data points are fitted with log-polynomial functions to migrate the effect of the statistical fluctuations while preserving possible energy dependent structures.

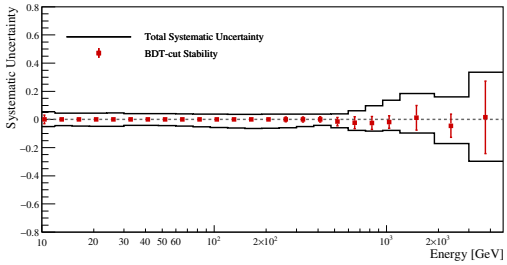

Figure 4: Energy dependence of systematic uncertainties. The red squares represent the average of all BDT training samples with respect to the standard 80% efficiency case, while the error bars represent the standard deviation at each energy bin.

Examples of BDT response distributions in the $754 < E < 959$ GeV bin and $1.5 < E < 4.8$ TeV bin including all acceptance conditions in shown in Fig. 2. In the final electron sample, the contamination ratios of protons are 5% up to 1 TeV, and less than 10% in the TeV region, while keeping a constant high efficiency of 80% for electrons after the pre-selection.

Systematic uncertainties Systematic errors include errors in the absolute normalization and energy dependent ones, except for the energy scale uncertainty. The energy dependent errors include those obtained from trigger efficiency in the low-energy region, tracking dependence, dependence on methods of charge identification and of electron identification, BDT stability, as well as MC model dependence. Figure 3 shows the energy dependence of systematic uncertainties in the tracking algorithms (electromagnetic shower tracking or Kalman filter tracking [13], charge selection (CHD or IMC), electron identification methods (K-estimator or BDT) and MC models (EPICS and Geant4. BDT stability is evaluated from the stability of the flux obtained with 100 independent training samples as a function of BDT cut efficiency in the range from 70% to 90% in 1% steps for each corresponding test sample. The red square in Fig. 4 represent the average of all BDT training sample with respect to the standard 80% efficiency case, while the error bars represent the standard deviation at each energy bin. The upper and lower edge of the error bars taken as the total systematic uncertainty due to the BDT analysis.

4. Results

The differential flux $\Phi(E)$ [$m^{-2}sr^{-1}s^{-1}GeV^{-1}$] between E and $E + \Delta E$ [GeV], with bin width ΔE [GeV], is given the following formula:

$$\Phi(E) = \frac{N(E) - N_{\rm BG}(E)}{S\Omega\varepsilon(E)T(E)\Delta E(E)} \tag{1}$$

where N is the number of electron candidates in the corresponding bin, $N_{\rm BG}$ is the number of background events estimated with MC protons, $S\Omega$ [m^2sr] is the geometrical acceptance, $\varepsilon(E)$ is the detection efficiency for electrons defined as the product of trigger, preselection, track reconstruction, and electron identification efficiencies, and $T(E)$ [sec] is the observational live time. While $T(E)$ is

PoS(ICRC2023)071

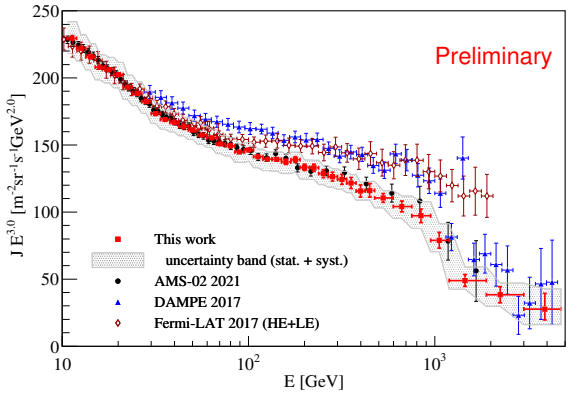

Figure 5: Cosmic-ray electron + positron spectrum observed with CALET, where the gray band indicates the quadratic sum of statistical and systematic errors. Also plotted are other direct measurements in space [14–16]. The horizontal error bars are representative the bin width.

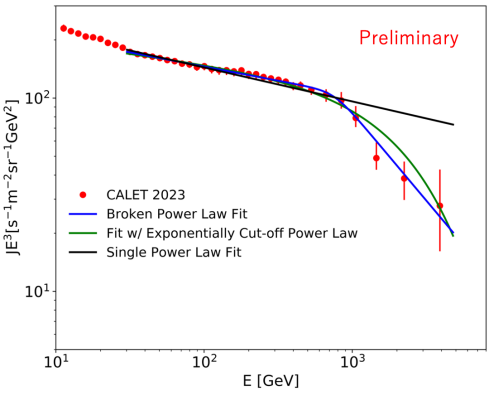

Figure 6: All-electron spectrum measured by CALET, and the fitted results in the energy range from 30 GeV to 4.8 TeV, with a broken power law, an exponentially cutoff power law and a single power law. The error bars represent statistical and systematic uncertainties except normalization.

basically energy independent, at lower energies it is reduced because we only use data taken below 6 GV cutoff rigidity.

Figure 5 shows the all-electron spectrum obtained in this analysis using the observed events with statistics increased by a factor 3.4 since the last publication [7]. The error bars along the horizontal and vertical axes indicate the bin width and statistical errors, respectively. The gray band is representative of the quadratic sum of statistical and systematic errors.

Comparing the other space experiments (Fermi-LAT, AMS-02 and DAMPE), the CALET spectrum shows good agreement with AMS-02 data up to 2 TeV. In the energy region from 30 to 300 GeV, the fitted power-law spectrum index, -3.14 ± 0.02, is roughly consistent with the values quoted by other experiments within the errors. However, the CALET spectrum appears to be softer compared to Fermi-LAT and DAMPE, and the flux measured by CALET is lower than that seen by Fermi-LAT and DAMPE, starting near 60 GeV and extending to near 1 TeV, indicating the presence of unknown systematic effects.

In Fig. 6 we fit the differential spectrum in the energy range from 30 GeV to 4.8 TeV with a smoothly broken power-law model [17]. The model is defined as; $J(E) = C(E/100\ \mathrm{GeV})^{\gamma}(1 + (E/E_b)^{\Delta\gamma/s})^{-s}$, where E_b is the break energy, while γ is the power index below E_b and $\Delta\gamma$ is the difference in the power low index below and above E_b. The fitted spectrum steepens from $\gamma = -3.15 \pm 0.01$ by $\Delta\gamma = -0.77 \pm 0.22$ at energy $E_b = 761 \pm 115$ GeV with the break smoothness parameter, s, fixed to 0.12 which fits our data well, with $\chi^2 = 3.6$ and 27 degrees of freedom (NDF). A single power-law fit gives $\gamma = -3.18 \pm 0.01$ with χ^2/NDF= 56/29, which means that a broken power law is favored with 6.9σ significance over a single power law. An exponentially cutoff power law [14] with a power index of -3.10±0.01 below a cutoff energy of 2854±305 GeV fits also our data well, with $\chi^2/\mathrm{NDF} = 12/28$ and a significance of 6.6σ over the single power law.

PoS(ICRC2023)071

5. Summary

We have updated our previous result [7] of the CALET all-electron spectrum with an approximate increase of the statistics more than 3. In the TeV region the data show a break of the spectrum compatible with the DAMPE results. The accuracy of determining the break's sharpness and position, and of the spectral shape above 1 TeV, are improved by the better statistics.

Extended CALET operations approved by JAXA in March 2021 through the end of 2024 (at least) with bring a further increase of the statistics and reduction of the systematic errors based on the analysis.

Acknowledgements

We gratefully acknowledge JAXA's contributions to the development of CALET and to the operations onboard the International Space Station. The CALET effort in Italy is supported by ASI ander Agreement No.2013-018-R.0 and its amendments. The CALET effort in the United States is supported by NASA through Grants No. 80NSSC20K0397, No. 80NSSC20K0399, and NNH18ZDA001N-APRA18-0004. This work is supported by JSPS KAKENHI Grant Numbers 19H05608 and 21K03592 in Japan.

References

[1] J. Nishimura *et al.*, Astrophys. J. **238**, 394 (1980)

[2] T. Kobayashi *et al.*, Astrophys. J. **601**, 340 (2004)

[3] O. Adriani *et al.* (PAMELA Collaboration), Nature **458**, 607 (2009)

[4] L. Accardo *et al.* (AMS-02 Collaboration), Phys. Rev. Lett. **113** 121101 (2014)

[5] S .Torii *et al.* (CALET Collaboration), Adv. Sp. Res. **64** 2531 (2019)

[6] O. Adriani *et al.* (CALET Collaboration), Phys. Rev. Lett. **119** 181101 (2017)

[7] O. Adriani *et al.* (CALET Collaboration), Phys. Rev. Lett. **120** 261102 (2018)

[8] Y. Asaoka, S. Ozawa, S. Torii *et al.* (CALET Collaboration), Astropart. Phys. **100** 29 (2018)

[9] K. Kasahara, EPICS, http://cosmos.n.kanagawa-u.ac.jp/EPICSHome/

[10] S. Roesler, R. Engel, and J. Ranft, DPMJET3, http://sroesler.web.cern.ch/sroesler/dpmjet3.html

[11] Y. Akaike *et al.* Proc. of 33rd ICRC, 726 (2013)

[12] Y. Asaoka, Y. Akaike *et al.* (CALET Collaboration), Astropart. Phys. **91** 1 (2017)

[13] P. Maestro *et al.* PoS(ICRC2017, 207 (2017)

[14] S. Abdollahi *et al.* (Fermi-LAT Collaboration), Phys. Rev. D **95** 082007 (2017)

PoS(ICRC2023)071

[15] M. Aguilar *et al.* (AMS-02 Collaboration), Phys. Rep. **894** 1 (2021)

[16] G. Ambrosi *et al.* (DAMPE Collaboration), Nature **552**, 63 (2017)

[17] M. Aguilar *et al.* (AMS-02 Collaboration), Phys. Rev. Lett. **114**, 171103 (2015)

PoS(ICRC2023)071

Full Authors List: CALET Collaboration

O. Adriani[1,2], Y. Akaike[3,4], K. Asano[5], Y. Asaoka[5], E. Berti[2,6], G. Bigongiari[7,8], W.R. Binns[9], M. Bongi[1,2], P. Brogi[7,8], A. Bruno[10], N. Cannady[11,12,13], G. Castellini[6], C. Checchia[7,8], M.L. Cherry[14], G. Collazuol[15,16], G.A. de Nolfo[10], K. Ebisawa[17], A.W. Ficklin[14], H. Fuke[17], S. Gonzi[1,2,6], T.G. Guzik[14], T. Hams[11], K. Hibino[18], M. Ichimura[19], K. Ioka[20], W. Ishizaki[5], M.H. Israel[9], K. Kasahara[21], J. Kataoka[22], R. Kataoka[23], Y. Katayose[24], C. Kato[25], N. Kawanaka[20], Y. Kawakubo[14], K. Kobayashi[3,4], K. Kohri[26], H.S. Krawczynski[9], J.F. Krizmanic[12], P. Maestro[7,8], P.S. Marrocchesi[7,8], A.M. Messineo[8,27], J.W. Mitchell[12], S. Miyake[28], A.A. Moiseev[29,12,13], M. Mori[30], N. Mori[2], H.M. Motz[18], K. Munakata[25], S. Nakahira[17], J. Nishimura[17], S. Okuno[18], J.F. Ormes[31], S. Ozawa[32], L. Pacini[2,6], P. Papini[2], B.F. Rauch[9], S.B. Ricciarini[2,6], K. Sakai[11,12,13], T. Sakamoto[33], M. Sasaki[29,12,13], Y. Shimizu[18], A. Shiomi[34], P. Spillantini[1], F. Stolzi[7,8], S. Sugita[33], A. Sulaj[7,8], M. Takita[5], T. Tamura[18], T. Terasawa[5], S. Torii[3], Y. Tsunesada[35,36], Y. Uchihori[37], E. Vannuccini[2], J.P. Wefel[14], K. Yamaoka[38], S. Yanagita[39], A. Yoshida[33], K. Yoshida[21], and W.V. Zober[9]

[1]Department of Physics, University of Florence, Via Sansone, 1 - 50019, Sesto Fiorentino, Italy, [2]INFN Sezione di Firenze, Via Sansone, 1 - 50019, Sesto Fiorentino, Italy, [3]Waseda Research Institute for Science and Engineering, Waseda University, 17 Kikuicho, Shinjuku, Tokyo 162-0044, Japan, [4]JEM Utilization Center, Human Spaceflight Technology Directorate, Japan Aerospace Exploration Agency, 2-1-1 Sengen, Tsukuba, Ibaraki 305-8505, Japan, [5]Institute for Cosmic Ray Research, The University of Tokyo, 5-1-5 Kashiwa-no-Ha, Kashiwa, Chiba 277-8582, Japan, [6]Institute of Applied Physics (IFAC), National Research Council (CNR), Via Madonna del Piano, 10, 50019, Sesto Fiorentino, Italy, [7]Department of Physical Sciences, Earth and Environment, University of Siena, via Roma 56, 53100 Siena, Italy, [8]INFN Sezione di Pisa, Polo Fibonacci, Largo B. Pontecorvo, 3 - 56127 Pisa, Italy, [9]Department of Physics and McDonnell Center for the Space Sciences, Washington University, One Brookings Drive, St. Louis, Missouri 63130-4899, USA, [10]Heliospheric Physics Laboratory, NASA/GSFC, Greenbelt, Maryland 20771, USA, [11]Center for Space Sciences and Technology, University of Maryland, Baltimore County, 1000 Hilltop Circle, Baltimore, Maryland 21250, USA, [12]Astroparticle Physics Laboratory, NASA/GSFC, Greenbelt, Maryland 20771, USA, [13]Center for Research and Exploration in Space Sciences and Technology, NASA/GSFC, Greenbelt, Maryland 20771, USA, [14]Department of Physics and Astronomy, Louisiana State University, 202 Nicholson Hall, Baton Rouge, Louisiana 70803, USA, [15]Department of Physics and Astronomy, University of Padova, Via Marzolo, 8, 35131 Padova, Italy, [16]INFN Sezione di Padova, Via Marzolo, 8, 35131 Padova, Italy, [17]Institute of Space and Astronautical Science, Japan Aerospace Exploration Agency, 3-1-1 Yoshinodai, Chuo, Sagamihara, Kanagawa 252-5210, Japan, [18]Kanagawa University, 3-27-1 Rokkakubashi, Kanagawa, Yokohama, Kanagawa 221-8686, Japan, [19]Faculty of Science and Technology, Graduate School of Science and Technology, Hirosaki University, 3, Bunkyo, Hirosaki, Aomori 036-8561, Japan, [20]Yukawa Institute for Theoretical Physics, Kyoto University, Kitashirakawa Oiwake-cho, Sakyo-ku, Kyoto, 606-8502, Japan, [21]Department of Electronic Information Systems, Shibaura Institute of Technology, 307 Fukasaku, Minuma, Saitama 337-8570, Japan, [22]School of Advanced Science and Engineering, Waseda University, 3-4-1 Okubo, Shinjuku, Tokyo 169-8555, Japan, [23]National Institute of Polar Research, 10-3, Midori-cho, Tachikawa, Tokyo 190-8518, Japan, [24]Faculty of Engineering, Division of Intelligent Systems Engineering, Yokohama National University, 79-5 Tokiwadai, Hodogaya, Yokohama 240-8501, Japan, [25]Faculty of Science, Shinshu University, 3-1-1 Asahi, Matsumoto, Nagano 390-8621, Japan, [26]Institute of Particle and Nuclear Studies, High Energy Accelerator Research Organization, 1-1 Oho, Tsukuba, Ibaraki, 305-0801, Japan, [27]University of Pisa, Polo Fibonacci, Largo B. Pontecorvo, 3 - 56127 Pisa, Italy, [28]Department of Electrical and Electronic Systems Engineering, National Institute of Technology (KOSEN), Ibaraki College, 866 Nakane, Hitachinaka, Ibaraki 312-8508, Japan, [29]Department of Astronomy, University of Maryland, College Park, Maryland 20742, USA, [30]Department of Physical Sciences, College of Science and Engineering, Ritsumeikan University, Shiga 525-8577, Japan, [31]Department of Physics and Astronomy, University of Denver, Physics Building, Room 211, 2112 East Wesley Avenue, Denver, Colorado 80208-6900, USA, [32]Quantum ICT Advanced Development Center, National Institute of Information and Communications Technology, 4-2-1 Nukui-Kitamachi, Koganei, Tokyo 184-8795, Japan, [33]College of Science and Engineering, Department of Physics and Mathematics, Aoyama Gakuin University, 5-10-1 Fuchinobe, Chuo, Sagamihara, Kanagawa 252-5258, Japan, [34]College of Industrial Technology, Nihon University, 1-2-1 Izumi, Narashino, Chiba 275-8575, Japan, [35]Graduate School of Science, Osaka Metropolitan University, Sugimoto, Sumiyoshi, Osaka 558-8585, Japan, [36]Nambu Yoichiro Institute for Theoretical and Experimental Physics, Osaka Metropolitan University, Sugimoto, Sumiyoshi, Osaka 558-8585, Japan, [37]National Institutes for Quantum and Radiation Science and Technology, 4-9-1 Anagawa, Inage, Chiba 263-8555, Japan, [38]Nagoya University, Furo, Chikusa, Nagoya 464-8601, Japan, [39]College of Science, Ibaraki University, 2-1-1 Bunkyo, Mito, Ibaraki 310-8512, Japan

PoS(ICRC2023)071